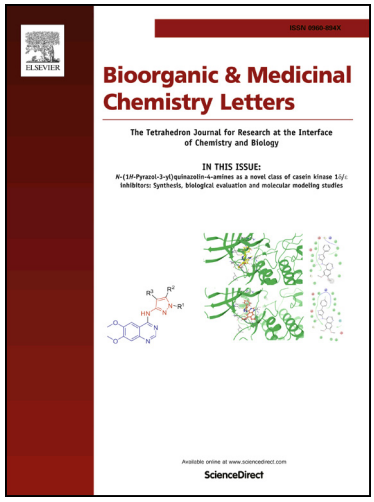

The Discovery of Benzoxazine Sulfonamide Inhibitors of $Na_V1.7$: Tools that Bridge Efficacy and Target Engagement

Daniel S. La, Emily A. Peterson, Christiane Bode, Alessandro A. Boezio, Howard Bregman, Margaret Y. Chu-Moyer, James Coats, Erin F. DiMauro, Thomas A. Dineen, Bingfan Du, Hua Gao, Russell Graceffa, Hakan Gunaydin, Angel Guzman-Perez, Robert Fremeau Jr., Xin Huang, Christopher Ilch, Thomas J. Kornecook, Charles Kreiman, Joseph Ligutti, Min-Hwa Jasmine Lin, Jeff S. McDermott, Isaac Marx, David J. Matson, Stefan I. McDonough, Bryan D. Moyer, Hanh Nho Nguyen, Kristin Taborn, Violeta Yu, Matthew M. Weiss

PII: S0960-894X(17)30568-1
DOI: http://dx.doi.org/10.1016/j.bmcl.2017.05.070
Reference: BMCL 25015

To appear in: *Bioorganic & Medicinal Chemistry Letters*

Received Date: 19 April 2017
Revised Date: 22 May 2017
Accepted Date: 23 May 2017

Please cite this article as: La, D.S., Peterson, E.A., Bode, C., Boezio, A.A., Bregman, H., Chu-Moyer, M.Y., Coats, J., DiMauro, E.F., Dineen, T.A., Du, B., Gao, H., Graceffa, R., Gunaydin, H., Guzman-Perez, A., Fremeau, R. Jr., Huang, X., Ilch, C., Kornecook, T.J., Kreiman, C., Ligutti, J., Jasmine Lin, M-H., McDermott, J.S., Marx, I., Matson, D.J., McDonough, S.I., Moyer, B.D., Nho Nguyen, H., Taborn, K., Yu, V., Weiss, M.M., The Discovery of Benzoxazine Sulfonamide Inhibitors of $Na_V1.7$: Tools that Bridge Efficacy and Target Engagement, *Bioorganic & Medicinal Chemistry Letters* (2017), doi: http://dx.doi.org/10.1016/j.bmcl.2017.05.070

The Discovery of Benzoxazine Sulfonamide Inhibitors of $Na_V1.7$: Tools that Bridge Efficacy and Target Engagement

Daniel S. La,[a] *Emily A. Peterson,*[a] *Christiane Bode,*[a] *Alessandro A. Boezio,*[a] *Howard Bregman,*[a] *Margaret Y. Chu-Moyer,*[a] *James Coats,*[a] *Erin F. DiMauro,*[a] *Thomas A. Dineen,*[a] *Bingfan Du,*[a] *Hua Gao,*[b] *Russell Graceffa,*[a] *Hakan Gunaydin,*[b] *Angel Guzman-Perez,*[a] *Robert Fremeau Jr.,*[d] *Xin Huang,*[b] *Christopher Ilch,*[d] *Thomas J. Kornecook,*[e] *Charles Kreiman,*[a] *Joseph Ligutti,*[II] *Min-Hwa Jasmine Lin,*[c] *Jeff S. McDermott,*[d] *Isaac Marx,*[a] *David J. Matson,*[d] *Stefan I. McDonough,*[d] *Bryan D. Moyer,*[e] *Hanh Nho Nguyen,*[a] *Kristin Taborn,*[d] *Violeta Yu,*[d] *Matthew M. Weiss*[a]

[a]Department of Medicinal Chemistry, [b]Department of Molecular Engineering, [c]Department of Pharmacokinetics and Drug Metabolism, and [d]Department of Neuroscience, Amgen Inc., 360 Binney Street, Cambridge, Massachusetts 02142, and [e]Department of Neuroscience, Amgen Inc., One Amgen Center Drive, Thousand Oaks, California 91320, United States

Abstract

The voltage-gated sodium channel $Na_V1.7$ has received much attention from the scientific community due to compelling human genetic data linking gain- and loss-of-function mutations to pain phenotypes. Despite this genetic validation of $Na_V1.7$ as a target for pain, high quality pharmacological tools facilitate further understanding of target biology, establishment of target coverage requirements and subsequent progression into the clinic. Within the sulfonamide class of inhibitors, reduced potency on rat $Na_V1.7$ versus human $Na_V1.7$ was observed, rendering in vivo rat pharmacology studies challenging. Herein, we report the discovery and optimization of novel benzoxazine sulfonamide inhibitors of human, rat and mouse $Na_V1.7$ which enabled pharmacological assessment in traditional behavioral rodent models of pain and in turn, established a connection between formalin-induced pain and histamine-induced pruritus in mice. The latter represents a simple and efficient means of measuring target engagement.

Chronic pain is a significant unmet medical need that remains unaddressed by current therapies which often do not provide adequate pain relief and carry significant undesirable side effects. It has been shown that humans with gain-of-function mutations in the gene that encodes for the voltage-gated sodium channel $Na_V1.7$, SCN9A, experience enhanced pain sensation whereas loss-of-function mutations lead to the inability to sense pain.[1] Accordingly, $Na_V1.7$ has become a highly pursued target within the biopharmaceutical industry as human genetics provide a compelling rationale that target engagement with an inhibitor would translate to pain relief in the clinic.

$Na_V1.7$ is a transmembrane (TM) voltage-gated sodium channel consisting of a 260 kDa pore-forming subunit. $Na_V1.7$ consists of 24 transmembrane helices over four domains (DI-DIV), in which each domain is comprised of six TM segments (S1-S6). The S5-S6 segments from each domain create the pore module of the channel and the S1-S4 segments form the voltage-sensing domain (VSD). A recent report from Genentech revealing an X-ray crystal structure of a sulfonamide small molecule ligand bound to a human $Na_V1.7$ bacterial Na_VAb channel chimera clearly pinpointed the binding site of this chemical class in the external cleft of VSDIV.[2] This structural elucidation is consistent with chimera studies from Pfizer and Amgen which also map the binding site of sulfonamide inhibitors to the VSDIV.[3] This class of sulfonamide inhibitors is of particular importance because it is one of the few chemical series that has been reported to consistently demonstrate high selectivity over Na_V isoforms, particularly, $Na_V1.5$, which is expressed in cardiac muscle and presents a significant off-target liability. Despite this inherent selectivity advantage, optimization of pharmacokinetics to afford adequate *in vivo* tools to evaluate target engagement and efficacy has been challenging. In this report, we highlight a benzoxazine sulfonamide inhibitor as a tool compound that show efficacy in both rat and mouse models of formalin-induced pain as well as a histamine-induced pruritus model in mice. With a single molecule, we thereby demonstrate $Na_V1.7$ target engagement in vivo and further support a link between behavior models of pain and itch. Furthermore, this finding enables the field, with greater confidence, to take

advantage of the histamine model as a measure of target of engagement which was been the cornerstone of our in vivo assessment of compounds in a practical and timely fashion.

We and others have previously reported $Na_V1.7$ inhibitors from several different structural classes[4] and more recently we have focused on acylsulfonamides[5] and bicyclic sulfonamides such as **1** (Scheme 1).[6] Early bicyclic sulfonamide inhibitors, whilst selective over $Na_V1.5$, have suffered from poor pharmacokinetic properties, demonstrating poor passive permeability and high rat in vivo clearance (Table 1).[7] Attempts to validate early leads from this class in rodent pain models, such as the rat formalin model, were unsuccessful due to weak inhibition of rat $Na_V1.7$ and the inability to achieve adequate target coverage.

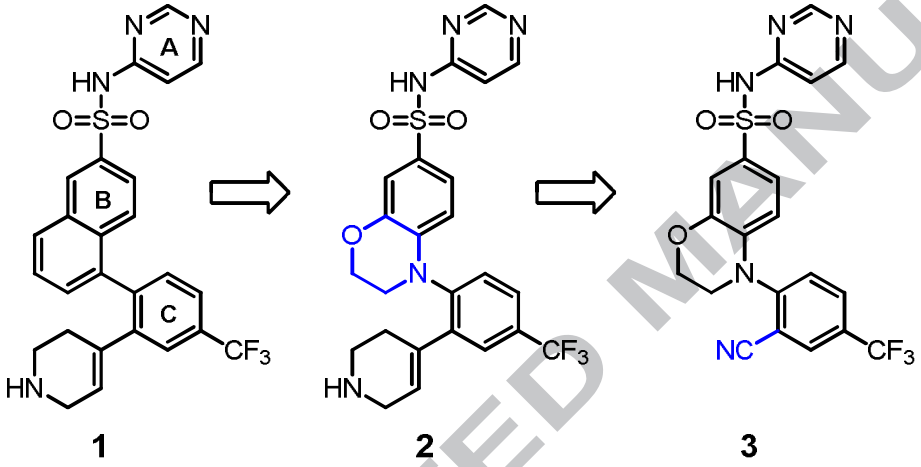

Scheme 1. Progression of bicyclic sulfonamide scaffolds

In addition to the lack of in vivo efficacy in rat for compounds such as **1**, the high lipophilicity and planar, aromatic nature of these molecules were also concerning, as both of these parameters often correlate with higher attrition.[8] In an effort to enter more "drug-like" chemical space, benzoxazine **2** was synthesized (Table 1). This new bicyclic scaffold had reduced lipophilicity and planarity, maintained modest $Na_V1.7$ potency and while it demonstrated reduced levels of selectivity over $Na_V1.5$ it did exhibit slightly improved unbound clearance (CLu) in rat. Similar to naphthalene **1**, benzoxazine **2** demonstrated poor passive permeability, presumably due to the basic amine present in the tetrahydropyridine and the resulting zwitterionic nature. A systematic scanning with chemical libraries of 2,4-disubstituted aryl C-rings led to the removal of the basic amine and

identification of more efficient analogs such as **3** with decreased lipophilicity, logD and molecular weight with respect to **1**.[9] Compound **3** had improved permeability and PK properties albeit with moderately decreased potency on human $Na_v1.7$.[10] A hypothesis detailing differences in residues about the binding pocket will be provided to account for the observed reduced potency on rat $Na_v1.5$ (vide infra).

Table 1. Improved permeability and PK as a result of truncated benzoxazine core

Compound	$hNa_v1.7$ PX IC_{50} (μM)	$rNa_v1.7$ PX IC_{50} (μM)	$Na_v1.5$ PX IC_{50} (μM) [fold over Nav1.7]	Rat IV CL [CLu] [a] (L/hr/kg)	P_{app} (μcm/s) [b]	cLog D (pH7.4)	LLE	MW
1	0.090	>30	>30 [>330x]	1.7 [40]	1.3	0.69	2.0	511
2	0.14	>30	1.5 [11X]	2.6 [14]	1.0	-1.4	2.6	518
3	0.46	3.0	4.6 [10x]	0.17 [7]	9.7	-0.2	2.5	461

[a] Clearance unbound was calculated by dividing rat clearance by unbound fraction as determined by equilibrium dialysis. 0.5 mg/kg as a solution in DMSO to male rats. CLu = clearance unbound. [b] P_{app} = passive permeability, LLE = ligand lipophilicity efficiency. MW = molecular weight. MDCK vector control, (A→B + B→A) /2.

In an effort to improve the potency of benzoxazine **3**, different heterocyclic sulfonamide A-rings were investigated within the context of the newly discovered benzoxazine core (Table 2). Although 1,2,4-thiadiazole **4** was the most potent inhibitor of $Na_V1.7$, permeability decreased with this heterocycle. 4-Amino-thiazole **7** demonstrated the best passive permeability of the heterocycles examined, but the potency was reduced in relation to **3** and many of the other heterocycles evaluated. With the exception of compound 7 all of the compounds demonstrated low turnover in both human and rat liver microsomes (HLM/RLM). Other five-membered ring heterocycles, represented by 2-aminooxazole **6** and 5-aminoisoxazole **8**, also resulted in significantly diminished potency and were not investigated further. In addition, the pKa of the sulfonamide nitrogen and therefore the population existing in the anionic state responsible for binding did not correlate with $Na_V1.7$ inhibition as the experimental pKa's for **3**, **4**, and **5** were 5.8, 3.8, and 7.0 respectively.[11] Despite it's potential for the formation of reactive metabolites, the 2-aminothiazole **5** provided the best balance of permeability, unbound clearance and potency on human $Na_V1.7$ and was therefore, kept constant for subsequent optimization.[12] The identification of a suitable replacement for the

2-aminothiazole, which lacked the inherent reactivity associated with this moiety, provided a significant challenge that could not be overcome within the context of this particular class of molecules.

Table 2. Exploration of the heterocyclic A-ring

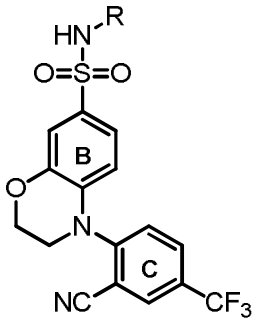

Compound	A-ring	hNa$_v$1.7 PX IC_{50} (μM)	RLM / HLM (μL/(min•mg))	Ave P_{app} (μcm/s)[a]	Rat IV CL [CLu] (L/hr/kg)[b]
3	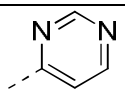	0.46	<14 / <14	9.7	0.17 [7]
4	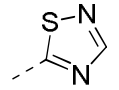	0.09	<14 / 34	1.6	0.64 [71]
5	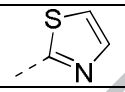	0.19	<14 / <14	22	0.33 [31]
6	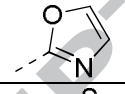	2.6	15 / <14	6.4	ND
7	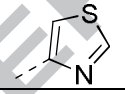	2.8	55 / <14	39	ND
8	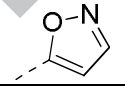	9.2	32 / <14	<1	ND

[a] P_{app} = passive permeability, MDCK vector control, (A→B + B→A) /2. [b] Clearance unbound was calculated by dividing rat clearance by unbound fraction as determined by equilibrium dialysis. 0.5 mg/kg as a solution in DMSO to male rats. CLu = clearance unbound.

Efforts next shifted to the C-ring portion of the molecule (Table 3). Using insight from previously reported SAR,[6] the majority of the substitutions explored were centered upon the 2- and 4-positions of the C-ring. With

the aim of identifying compounds with suitable pharmacokinetics to enable oral dosing in appropriate pharmacodynamics and/or efficacy models, attention focused on improving the potency while maintaining low turnover in liver microsomes and good passive permeability. The most potent human $Na_v1.7$ inhibitors contained lipophilic groups at C4, such as CF_3 (see **5** and **9**). The 2-position of the C-ring was tolerant of a wide variety of substitution and it was found that a methoxy group provided a good balance across the parameters being evaluated. In an attempt to mitigate the higher log D, the *ortho*-OMe group was paired with either a nitrile, a hydrogen or a fluorine at the *para* position to give **10** – **12**. These compounds demonstrated the best combination of potency on $Na_V1.7$ and selectivity over $Na_V1.5$. Unfortunately, **11** and **12** demonstrated high turnover in both human and rat liver microsomes, thereby limiting their utility moving forward.

Table 3. Exploration of C-Ring SAR

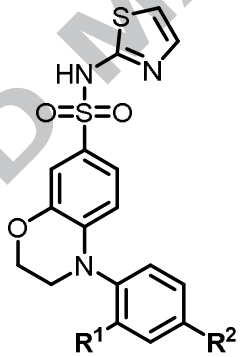

Compound	R^1	R^2	$hNa_v1.7$ PX IC_{50} (μM)	$rNa_v1.7$ PX IC_{50} (μM)	$Na_v1.5$ PX IC_{50} (μM) [fold]	Rat IV CL [CLu] (L/hr/kg) [a]	HLM / RLM (μL/(min• mg))	Ave P_{app} (μcm/s) [b]
5	CN	CF3	0.19	1.1	1.5 [8]	0.33 [31]	<14 / <14	22
9	OMe	CF3	0.12	0.39	2.0 [17]	0.24 [40]	30 / 53	32
10	OMe	CN	0.25	0.85	14 [56]	0.84 [53]	36 / 22	20
11	OMe	H	0.38	1.6	>30 [>79]	ND	68 / 297	28
12	OMe	F	0.28	0.88	>30 [>100]	ND	110 / >399	36

[a] Clearance unbound was calculated by dividing rat clearance by unbound fraction as determined by equilibrium dialysis. 0.5 mg/kg as a solution in DMSO to male rats. CLu = clearance unbound. [b] P_{app} = passive permeability, MDCK vector control, (A→B + B→A) /2.

Keeping the thiazole constant as the A-ring, susbstitution of the B-ring was also explored (Table 4). Despite the greater $Na_V1.5$ selectivity of **10**, the trifluormethyl C-ring substituent of **5** was chosen for further exploration given the greater body of historical data that existed with the 2-cyano-4-trifluromethyl C-ring which allowed for ease of comparison between analogs. Substitution of the aromatic portion of the benzoxazine B-ring revealed that although small electron-withdrawing groups could be tolerated, they did not dramatically alter potency, intrinsic stability (HLM / RLM) or the passive permeability. The position most tolerant to fluoro-substitution was R^6 (compare **13**, **14** and **15**). Within this series, the R^6 fluoro and chloro-analogs (**15** and **16)** led to diminished selectivity over $Na_V1.5$ as compared to compound **5**. Furthermore, as selectivity over $Na_V1.5$ eroded, the potency on rat $Na_V1.7$ was improved. Substitution of the sp^3-hybridized carbons linking the oxygen and nitrogen atoms of the benzoxazine ring was also investigated with groups such as methyl, ethyl, phenyl and carbonyl with no observed improvement in either potency or selectivity (data not shown).

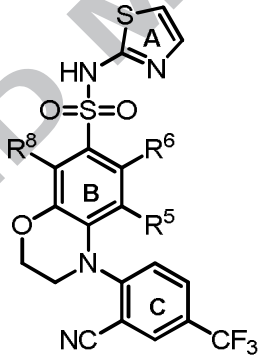

Table 4. Modification of the benzoxazine B-ring

Compound	R^5	R^6	R^8	$hNa_v1.7$ PX IC_{50} (μM)	$rNa_v1.7$ PX IC_{50} (μM)	$Na_v1.5$ PX IC_{50} (μM)	HLM / RLM (μL/(min•mg))	Ave P_{app} (μcm/s)[a]
5	H	H	H	0.19	1.1	1.5	<14 / <14	22
13	H	H	F	0.52	1.7	2.1	<14 / <14	38
14	F	H	H	2.0	0.56	0.65	<14 / <14	26
15	H	F	H	0.14	0.067	0.32	<14 / <14	19
16	H	Cl	H	0.39	0.05	0.61	22 / 21	27

[a] P_{app} = passive permeability, MDCK vector control, (A→B + B→A) /2.

The recent advancement in $Na_V1.7$ structural biology enables a closer examination of ligand/protein interaction, providing insight into the origins of potency and varying selectivity over $rNa_V1.7$.[2] Genentech

obtained an X-ray structure of **17** (GX-936, Figure 1A)[13] bound to a $Na_v1.7$ bacterial Na_VAb channel chimera, clearly depicting the ligand/protein interactions within the VSDIV pocket. Binding of our sulfonamide benzoxazine inhibitors to this pocket was confirmed by a $hNa_V1.7$ radioligand binding assay employing a tritiated ligand[14] that is routinely displaced by compounds highly homologous to **17**. Employing this assay, bicyclic sulfonamides **1**, **4**, **15** and **16** were determined to have IC_{50} values equal to 0.030, 0.021, 0.037 and 0.020 μM respectively, suggesting that the binding site for these compounds and **17** is the same.[5] This data, in turn, enabled computational docking to understand the critical protein interactions with the benzoxazines.[15] Compounds **1**, **2** and **3** in their ionized states were docked into the VSDIV binding site of the reported structure. The acidic sulfonamide moiety engages Arg1602, Arg1608 and Asn1540 in an H-bonding network while additionally participating in a charge-charge interaction with Arg 1605 and Arg1608 as shown in the interaction map of Figure 1C and 3-dimensionally in Figure 2A. All four residues are conserved between $hNa_V1.7$, $rNa_V1.7$ and $hNa_V1.5$ (Table 5 in blue). Critical to this series of key interactions is the two-point contact between Arg1608 and both the deprotonated sulfonamide nitrogen and the adjacent heterocyclic A-ring nitrogen (N at the 3-position on **2** see Figure 2B). Consistent with this sulfonamide binding mode, potency is lost with compound **8** where the 2-pyridyl A-ring is replaced by a 5-aminoisoxazole ring (N vs. O H-bond acceptor).

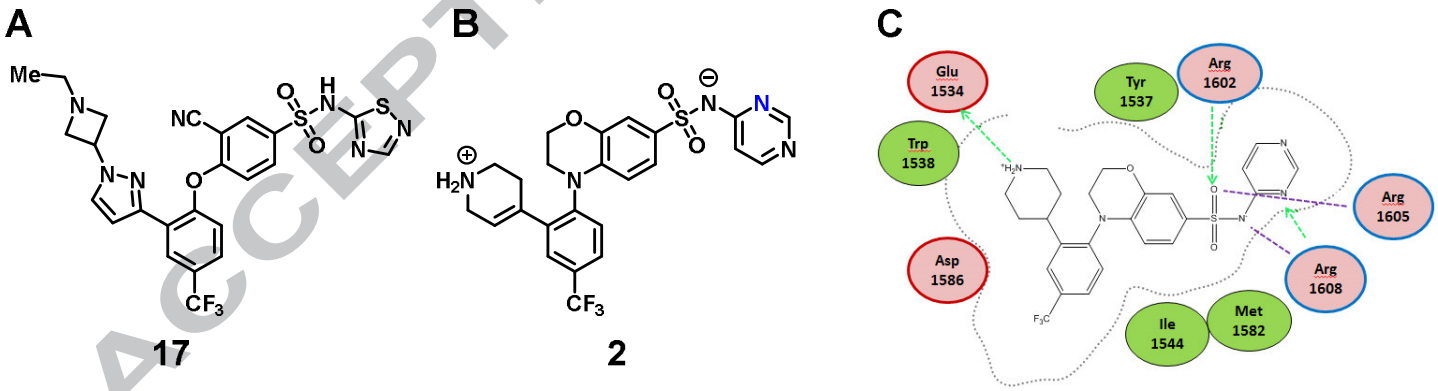

Figure 1. (A) Compound **17**, used by Genentech as a ligand for X-ray crystallography. (B) Docking with compound 2 performed in the ionized state. (C) Compound **2**-Protein interaction map. Pink circle: charged or H-bond interaction. Green circle: hydrophobic interaction. Purple dotted line: charge-charge interaction. Green dotted line: H-bond

Despite the high global homology between hNa$_V$1.7 and rNa$_V$1.7 (93%),[16] the selectivity of certain sulfonamides over rNa$_V$1.7 can be rationalized by the differences in residues surrounding the substituent at the *ortho*-position of the C-ring. For compounds **1** and **2**, no rat activity is observed (rNa$_V$1.7 IC$_{50}$ >30 μM). Glu1534 (Figures 1C and 2C), which is unique to hNa$_V$1.7 (Table 5), engages the basic tetrahydropyridine moiety. In contrast, rNa$_V$1.7 contains a tyrosine at the same position which cannot participate in this strong enthalpic interaction and may be electrostatically disfavored, consistent with the lack of rat activity. Proximal to Glu1534 on the same S2 helix is Tyr1537 which engages the ligand in a π-stacking interaction as shown in Figure 2C. Residues 1531 and 1533, which also differ amongst the proteins, reside on the same helix but do not directly engage the ligand, suggesting that the local environment could also playing a role in the observed levels of selectivity. rNa$_V$1.7 potency increases when the basic tetrahydropyridine is replaced by a smaller nitrile (**3**). The shorter nitrile of **3** can interact with Trp1538 (conserved in both human and rat) through either an H-bond with the indole NH or a π-π interaction.

Table 5. Selected residues from sequences alignments between hNa$_v$1.7 and rNa$_v$1.7. [a]

	1531	1533	1534	1537	1538	1540	1541	1587	1602	1605	1608
hNav1.7	His	Thr	Glu	Tyr	Trp	Asn	Val	Leu	Arg	Arg	Arg
rNav1.7	Tyr	Asp	Tyr	His	Trp	Asn	Met	Met	Arg	Arg	Arg

[a] Residues are highlighted in blue (conserved), red (directly interact with ligand) and black (further removed from ligand region)

The effect of halogenation of the benzoxazine core on enhancing rNa$_V$1.7 activity highlighted in Table 4 can be explained by the residue differences at position 1541 (Figure 2D and Table 5). Within range of R^6 (**15** and **16**, Table 4) Met1541 (in rat) extends beyond a shorter valine (human) and as a result, it could engage in either an enhanced van der Waals (VDW) contact or a halogen-bonding interaction. The VDW contact is consistent with the tolerance of the adjacent R^5 fluorine on compound **14** which is also proximal to Met1541.

The majority of residue differences residing proximal to the *ortho*-substituent on the C-ring highly implicates this region of the protein as the main driver of selectivity profile. These explanations for increased rNa_V1.7 potency, however, do not account for the changes in helix movement as these arguments are primarily rooted in residue differences in the DIV pocket that are in direct contact with the ligands. Despite the high sequence homology for human and rat, especially outside the immediate binding pocket, discrepancies at remote sites may also govern selectivity profile. For instance, Leu1587 is located on the S6 helix and remote form the binding site. This distal position is in stark contrast to the two other residues at 1531 and 1533 which are directly adjacent to those that make direct contact with the ligand (outer sphere residues are highlighted in black in Table 5.). While it is less clear how remote residue differences effect binding and protein movement, this analysis of proximal residue differences provides a rationale for binding and selectivity which in turn could enhance prospective design.

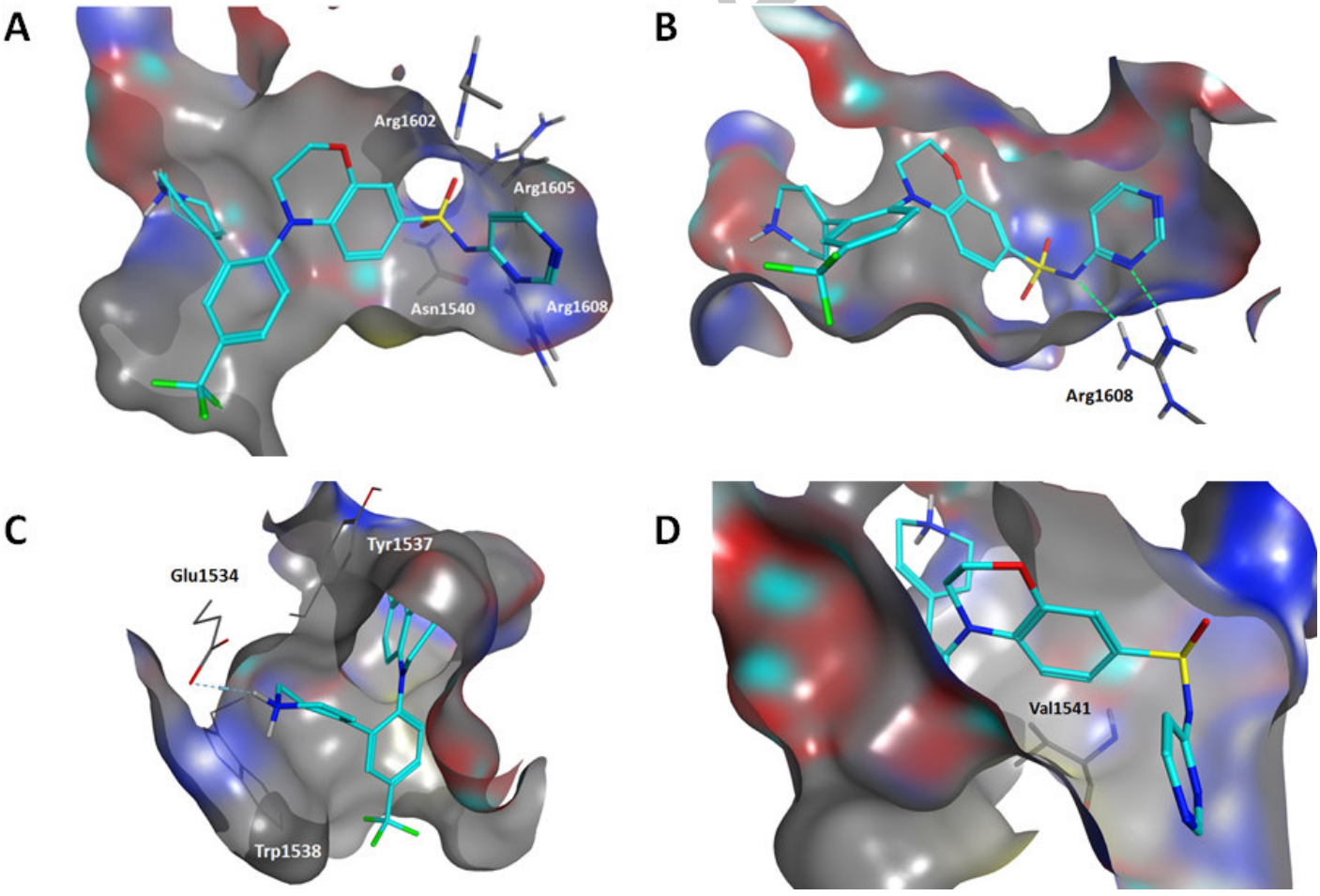

Figure 2. (A) Critical binding interaction between the sulfonamide moiety of compound **2** and surrounding charged arginine residues. (B) Critical 2-point interaction between Arg1608 and the sulfonamide moiety of compound **2** (C) D-Ring interactions with residues that govern rat and Nav1.5 selectivity. (D) Met1541 in rat (Val in human) is poised to interact with the R^5 and R^6 halogen.

Compounds **15** and **16** proved unique within the sulfonamide class due to their cross-species inhibition of $Na_v1.7$ and their ability to interrogate in vivo pharmacology associated with inhibitors that act through binding with the DIV pocket. As mentioned previously, inhibitors with aromatic bicyclic cores such as **1** did not show efficacy in the rat formalin pain model. Because of the significant homology between the human and rat $Na_V1.7$ channels (93% homology), it was anticipated that the sulfonamides would demonstrate similar potency for the inhibition of human and rat $Na_V1.7$; it was subsequently found that this was not the case. While the benzoxazines had diminished selectivity over $Na_V1.5$, the observation that these compounds demonstrated robust inhibition of rat $Na_v1.7$ was an unexpected and useful discovery because of the scaffold's potential to deliver valuable *in vivo* tools.

Although several rodent models of nociceptive pain are commonly used to assess analgesic efficacy,[17] our own prior experience,[4] as well as other reports of $Na_V1.7$ inhibitors blocking pain response in the rat formalin model,[18] prompted us to investigate a representative compound in the formalin assay.[19] Compound **15** was chosen to assess the efficacy of a sulfonamide $Na_V1.7$ inhibitor in a rat model of formalin-induced pain due to its potency on rat $Na_V1.7$ and its pharmacokinetic profile in rat (10 mg/kg PO dose: Cmax = 0.99 μM AUC = 20 μM•h, %F = 57, 0.5 mg/kg IV dose: CL [CLu] = 0.6 [39] L/h/kg, F_u = 0.015).[20] Compound **15** showed dose- and exposure-dependent efficacy in the formalin model, with statistically significant analgesic effects at 30 and 100 mg/kg (Figure 3A). The 30 mg/kg and 100 mg/kg doses produced 39 and 70% reductions in nociceptive behavior, respectively with unbound plasma coverage of 1.3 and 3.6-fold over the rat $Na_V1.7$ IC_{50} (See Table 6). We considered it very unlikely that formalin responses were due to inhibition of $Na_V1.8$, a tetrodotoxin-resistant (TTX-R) Nav isoform implicated in nociception and action potential electrogenesis,[21] since the IC_{50} for **15** to block TTX-R currents in rat dorsal root ganglion (DRG) neurons was >30 μM, when evaluated on closed or partially-inactivated channels, a concentration well above free drug concentrations achieved in our in vivo

studies. Notably, a previously reported $Na_V1.8$ inhibitor was found to be efficacious in models of neuropathic and inflammatory pain, but ineffective in a model of formalin-induced nociception. [22]

The difference in sulfonamide potency between human and rat $Na_V1.7$ prompted us to test potency across a broader species panel. Similar to a report published from Pfizer demonstrating the species- and isoform-selectivity of sulfonamide **18** (PF-04856264),[13] compound **1**, which was selective over human $Na_V1.5$, potently inhibited $Na_V1.7$ channels from cynomolgus monkey and mouse, but not rat (Table 6).[23] Compounds **15** and **16** demonstrated potent inhibition of both mouse and monkey $Na_V1.7$ channels and this observation enabled establishing a pharmacodynamic model in mice. In addition, compound **15** was further investigated in a mouse TTX-sensitive dorsal root ganglion electrophysiology assay and was found to be potent (IC_{50} of 53 nM). This potency correlates well with the mouse $Na_V1.7$ potency determined in our in vitro HEK assay and further reinforces the connectivity between mouse, rat and human activity. Since compound **15** demonstrated statistically significant analgesia in the rat formalin model, it was postulated that this molecule could be used to validate a similar pain model in mouse.

Table 6. Isoform and species selectivity profiles for selected compounds

Compound	human $Na_v1.7$ IC_{50} (μM)	cyno $Na_v1.7$ IC_{50} (μM)	mouse $Na_v1.7$ IC_{50} (μM)	rat $Na_v1.7$ IC_{50} (μM)	human $Na_v1.5$ IC_{50} (μM)
18	0.20 / 0.028[a]	0.02[a]	0.13[a]	4.2[a]	>30 / >10[a]
1	0.09	0.10	4.3	>30	>30
15	0.14	0.37	0.06	0.07	0.33
16	0.39	0.30	0.10	0.05	0.61

[a]Published data

When dosed orally in mice, **15** provided an acceptable pharmacokinetic profile (Cmax = 58 μM, AUC = 790 μM•h, $t_{1/2}$=7 h and F_u = 0.006) and it was anticipated that sufficient unbound plasma concentrations (C_u) could be achieved in order to enable informative in vivo pharmacology studies in mice (see Table 7.). To determine its analgesic effect in mice, **15** was dosed at 30, 60, and 100 mg/kg in C57BL/6 male mice and nociceptive (flinching and licking) behavior was measured after subcutaneous injection of formalin (2%) into the dorsal hind paw (Figure 3B). It was found that **15** demonstrated robust inhibition of formalin-induced pain

behavior in a dose-dependent fashion, with statistically significant effects at the 60 mg/kg (45% MPE) and 100 mg/kg (77% MPE) doses. The free plasma concentration multiple over mouse $Na_V1.7$ IC_{50} (C_u/m $Na_V1.7$ IC_{50}) required to elicit an analgesic effect in mouse formalin (16x) was slightly higher than that required to elicit a similar response it the rat formalin model (3.6x). The reasons for this modest difference in coverage requirements is currently unclear. (Figure 3A, Table 8). These results provided an important proof-of-concept for establishing a measure of efficacy in mouse for evaluating selective sulfonamide inhibitors.

Table 7. Rat and mouse PK of **15**

Species	Route (mg/kg)	AUC_{inf} (μM•h)	CL (L/h/kg)	$T_{1/2}$ (h)	Vd (L/kg)	C_{max} (μM)	Tmax (h)	F (%)	Plasma protein binding (%)
Rat	i.v. (0.5)	1.8	0.60	3.6	2.5				98.5
Rat	p.o. (10)	20		9.8		0.95	6.7	57	98.5
mouse	p.o. (30)	790		7.1		58	2.0		99.4

Despite success in demonstrating that the mouse formalin model is sensitive in detecting analgesic activity of our $Na_V1.7$ inhibitors, the labor-intensive nature of manually assessing formalin-induced pain behavior in mice led us to pursue a more sensitive and higher throughput pharmacodynamic model. In addition to its role in sensing pain stimuli, $Na_V1.7$ has also been implicated in the perception of itch. Some individuals with congenital insensitivity to pain (CIP) are also insensitive to itch, while others with gain-of-function mutations suffer from neuropathic itch.[24] Accordingly, we have found global $Na_V1.7$ knockout mice recapitulate the human CIP phenotype. In addition to the lack of response to chemical, mechanical and thermal pain stimuli, these knockout mice also exhibit no scratching response to an intra-dermal injection of histamine.[25]

Due to the underlying commonality between the neural anatomy responsible for conveying itch and pain information, it was hypothesized that a rodent itch model could provide a reliable means of estimating $Na_V1.7$ target engagement while also improving project process flow.[26] Toward this end, C57BL/6 male mice were dosed orally with 30, 60 or 100 mg/kg of **15** 120 minutes prior to receiving a challenge dose of histamine, a

known pruritogen. Histamine was administered intradermally to the nape of the neck immediately prior to testing and the number of resulting scratch bouts was measured over a 0-30 minute period. Gratifyingly, all three doses of **15** provided a statistically significant reduction in itch response compared to vehicle (Figure 3C).[27] The unbound concentration of the 30, 60 and 100 mpk doses were 0.37, 0.66 and 0.68 µM respectively, which corresponds to multiples of 6 – 11-fold over the mouse $Na_V1.7$ IC_{50} (Table 8). This data is consistent with that obtained in the mouse formalin assay in which the efficacious concentration at the 60 mg/kg dose (0.62 µM) was 10-fold over IC_{50}. The similarity in target coverage between the two models helped confirm for the first time in our program that a histamine-induced pruritis assay could be used as a model to assess target engagement. In turn, the development of this assay significantly streamlined in vivo assessment of future compounds that will be disclosed shortly.

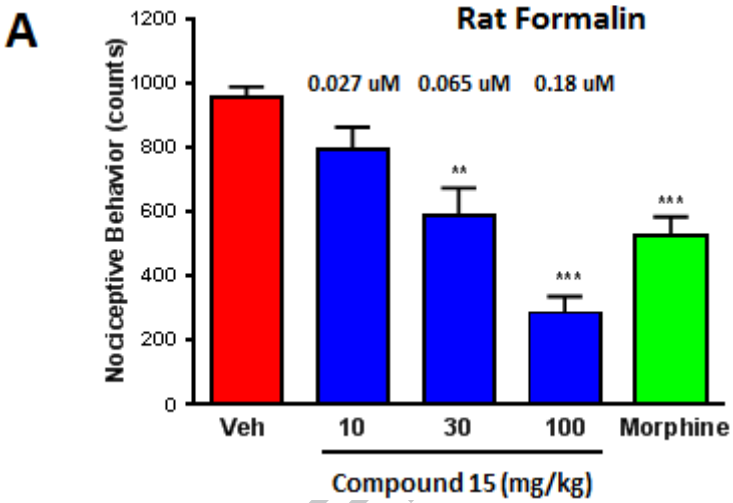

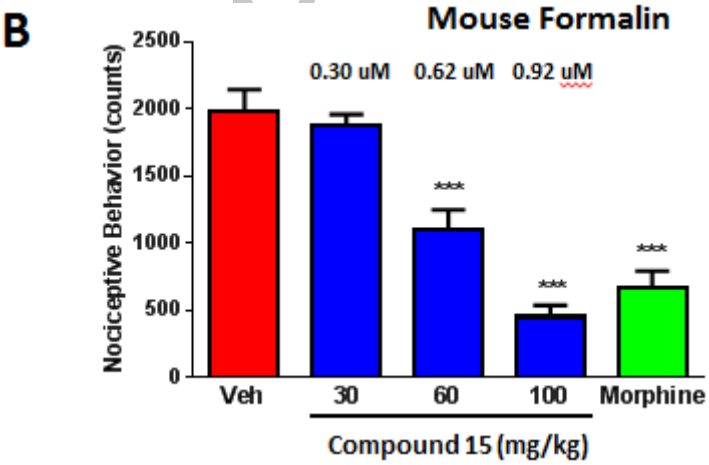

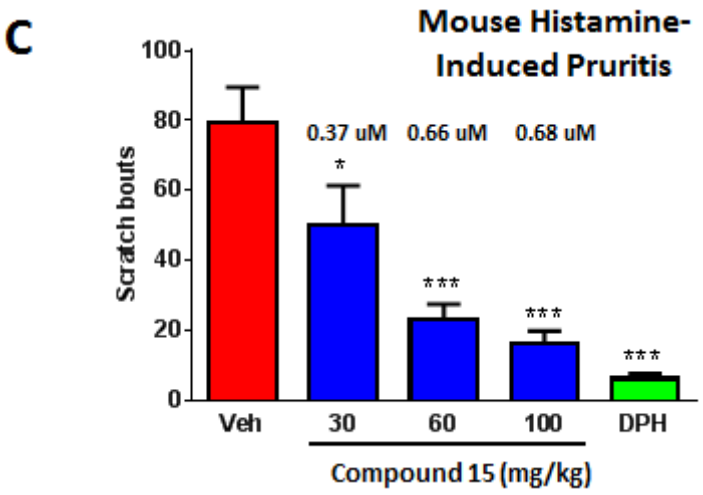

Figure 3. (A) Total phase II formalin-induced nociceptive behavior (flinches) in Sprague Dawley rats administered vehicle, morphine sulfate (subcutaneous dosing, 2 mg/kg), or 10, 30, or 100 mg/kg of **15** (PO, formulation: 30% (w/v) hydroxypropyl β-cyclodextrin in water pH adjusted to 10.0 with KOH). Unbound concentrations are expressed above bars. (B) Total phase II formalin-induced nociceptive behavior (paw licking and lifting) in C57Bl/6 mice administered vehicle, morphine sulfate (subcutaneous dosing, 3 mg/kg), or 30, 60, or 100 mg/kg of **15** (PO, formulation: 30% (w/v) hydroxypropyl β-cyclodextrin in water pH adjusted to 10.0 with KOH). Unbound concentrations are expressed above bars. (C) Effect of **15** on histamine-induced pruritus in C57BL/6 male mice administered vehicle, diphenhydramine (30 mg/kg; 90 min prior to test, PO, formulation: water), 30, 60, or 100 mg/kg of **15** (120 min prior to test, PO, formulation: 30% (w/v) hydroxypropyl β-cyclodextrin in water pH adjusted to 10.0 with KOH); y-axis: total number of scratch bouts over 30-min time period following histamine administration (8.15mM i.d.). Unbound concentrations are expressed above bars.

Table 8. Plasma exposure and unbound concentration target coverage

In Vivo Assay	Dose (mpk)	Mean Plasma Conc. (μM)	Cu/ rodent $Na_V1.7$ IC_{50}	Effect (%)
Rat Formalin	10	1.7	0.5	17
	30	4.2	1.3	39
	100	11	3.6	70
Mouse Formalin	30	51	5	5
	60	100	10	45
	100	150	16	77
Mouse Histamine Pruritis	30	61	6	37
	60	109	10	71
	100	113	11	80

The synthesis of key compounds **15** and **10** is illustrated below in Scheme 2. The syntheses of these benzoxazine inhibitors can be achieved by two complementary routes that allow late-stage structural modification of either the A- or C-rings. Route 1, which is exemplified by the synthesis of **15**, starts with S_NAr arylation of benzoxazine **17** with an appropriately functionalized fluoroarene such as **18** followed by chlorosulfonylation to provide sulfonyl chloride **20**. Sulfonamide formation proceeds upon mixing the heterocyclic amine **21** with the sulfonyl chloride and treating the mixture with LHMDS at 0 °C. Aqueous workup and treatment with trifluoroacetic acid provides inhibitors such as **15**.

Alternatively, for SAR exploration of the C-ring (Table 4), the synthesis using Route 2 started from commercially available sulfonyl chloride **22**, which after installation of the protected A-ring heterocyclic amine, underwent hydrolysis and subsequent reduction to give phenolic aniline **24**. Cyclization of **24** with chloroacetylchloride (**25**) followed by borane reduction of the lactam provided benzoxazine **26**, a useful late-stage intermediate for C-ring diversification. Palladium-catalyzed amination of bromide **27** followed by deprotection of the sulfonamide with trifluoroacetic acid afforded **10**.

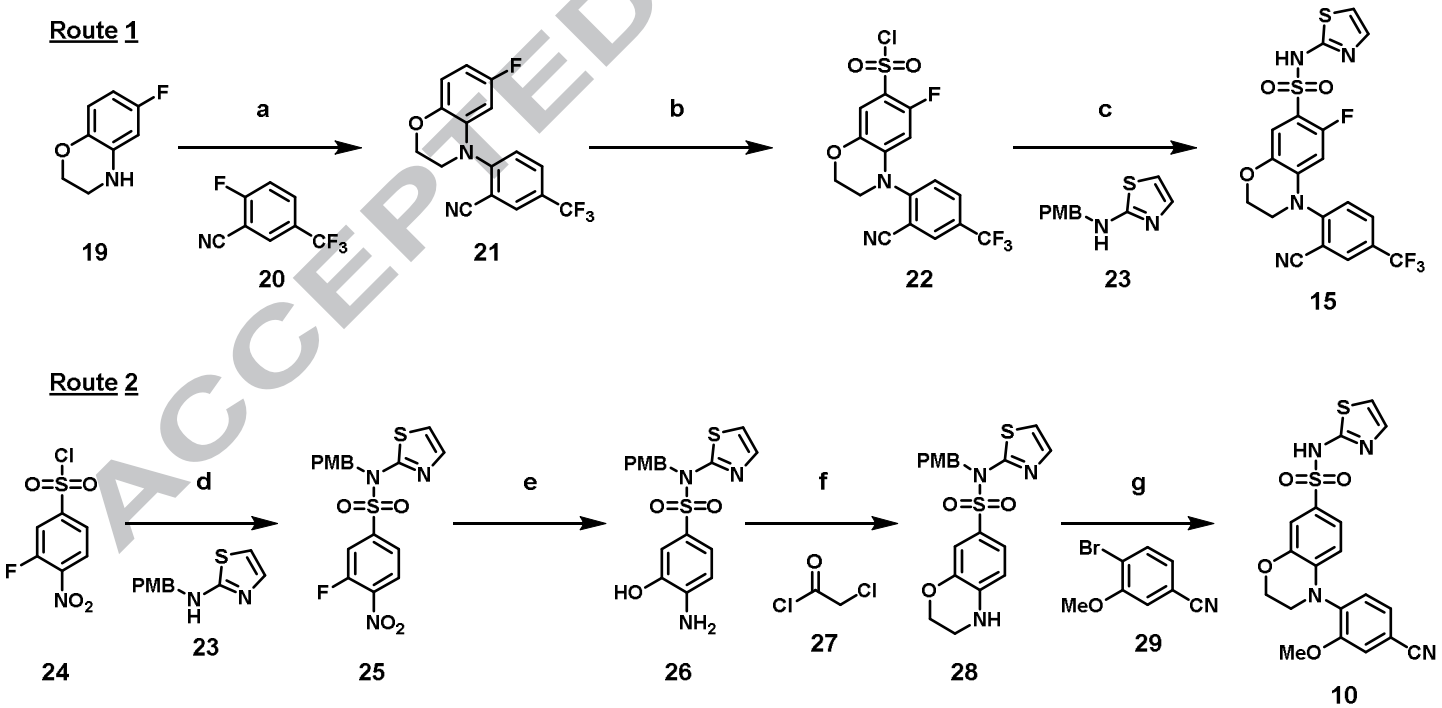

Scheme 2. Synthetic routes for the synthesis of benzoxazine $Na_v1.7$ inhibitors. Route 1: (a) NaH, THF, **20**, 0→60 °C, 63% (b) SO_2Cl_2, DCM, 0 °C, 75%; (c) i. LHMDS, THF, **23**, 0 °C→rt; ii. TFA, DCM, rt, 56% for 2 steps. Route 2: (d) LHMDS, THF, **23**, -78 °C, 73%; (e) i. NaOTMS, THF, 0 °C; ii. Fe, HOAc, THF, 70 °C, 92% yield over 2 steps; (f) i. **27**, K_2CO_3, DMF, 0-50 °C, 84%; ii. BH3•THF, THF, 0 °C, 78%; (g) **29**, XantPhos, $Pd_2(dba)_3$, NaO-*t*Bu, 130 °C, 56%.

In an attempt to improve upon the physical properties of the naphthalene–based Nav1.7 inhibitors represented by compound **1**, the benzoxazine class of inhibitors was synthesized to decrease planarity and reduce lipohilicity. Optimization of this scaffold led to the identification of an appropriate A-ring for improved permeability and in vivo clearance followed by recognition of a C-7 fluoride on the benzoxazine ring for improved rat potency. This work ultimately led to the discovery of **15**. The fortuitous rat potency and general disparity between rat and human activity are rationalized by docking studies employing the reported chimera X-ray structure. This in silico study highly implicates the region around the C-ring as critical to the selectivity profile. Compound **15** had sufficient exposure and rodent potency to progress to in vivo studies and demonstrate target coverage. **15** became a critical in vivo tool, for the first on our program, linking efficacy between a traditional model of pain sensitivity (formalin) and the histamine-induced pruritus assay in mouse. Although selectivity could be improved, the potential for cardiac toxicity due to $Na_V1.5$ inhibition precluded further investigation of this specific series for the development of a pain therapeutic. Nevertheless, the sulfonamide series was further optimized to related selective structures which will be the subject of future publications.

Supporting Information Available: In vitro and in vivo pharmacology assay protocols, PKDM assay protocols, synthetic experimental procedures, compound characterization.

Corresponding Author Information: Phone: 617-949-4131. Fax: 617-299-8379. E-mail: Daniel.la@sagerx.com

Author Information: Emily Peterson, Biogen Inc. Howard Bregman, Agios Pharmaceuticals. Erin DiMauro, Merck Inc. Thomas Dineen, Novartis AG. Bingfan Du, Mersana Therapeutics. Hakan Gunaydin, Merck Inc.

Robert Fremeau, NeuroRx Consulting. Jeff McDermott, Eli Lilly and Co. Isaac Marx, Biogen Inc. Stefan McDonough, Pfizer Inc. Hanh Nguyen, BlinkBio Inc.

Abbreviations Used: $Na_V1.7$, voltage gated sodium channel 1.7; SCN9A, sodium valtage-gated channel alpha subunit 9; TM, transmembrane; VSD, voltage sensing domain; CLu, unbound clearance; HLM, human liver microsome; RLM, rat liver microsome; PX, patch express; LLE, ligand lipophilicity efficiency. MW, molecular weight. MDCK, Madin-Darby canine kidney epithelial; SAR, structure activity relationship; VDW, van der Waals; MPE, maximal pharmacological effect; CIP, congenital insensitivity to pain

References and Notes

(1) (a) Faber, C. G.; Hoeijmakers, J. G. J.; Ahn, H.-S.; Checng, X.; Han, C.; Choi, J.-S.; Estacion, M.; Lauria, G.; Vanhoutte, E. K. Gerrits, M. M.; Dib-Hajj, S.; Drenth, J. P. H.; Waxman, S. G.; Merkies, I. S. J. Gain of function Nav1.7 mutations in idiopathic small fiber neuropathy. *Ann. Neurol.* **2012**, *71*, 26–39; (b) Dib-Hajj, S. D.; Binshtok, A. M.; Cummins, T. R.; Jarvis, M. F.; Samad, T.; Zimmermann, K. Voltage-gated soldium channels in pain states: Role in pathophysiology and targets for treatment. *Brain Res. Rev.* **2009**, *60*, 65–83. (c) Cox, J. J.; Reimann, F.; Nicholas, A. K.; Thornton, G.; Roberts, E.; Springell, K.; Karbani, G.; Jafri, H.; Mannan, J.; Raashid, Y.; Al-Gazali, L.; Hamamy, H.; Valente, E. M.; Gorman, S.; Williams, R.; McHale, D. P.; Wood, J. N.; Gribble, F. M.; Woods, C. G. An SCN9A channelopathy causes congenital inability to experience pain. *Nature* **2006**, *444*, 894–898. (d) Fertleman, C. R.; Baker, M. D.; Parker, K. A.; Moffatt, S.; Elmslie, F. V.; Abrahamsen, B.; Ostman, J.; Klugbauer, N.; Wood, J. N.; Gardiner, R. M.; Rees, M. SCN9A Mutations in paroxysmal clinical study extreme pain disorder: allelic variants underlie distinct channel defects and phenotypes. *Neuron* **2006**, *52*, 767–774. (e) Yang, Y.; Wang, Y.; Li, S.; Xu, Z.; Li, H.; Ma, L.; Fan, J.; Bu, D.; Liu, B.; Fan, Z.; Wu, G.; Jin, J.; Ding, B.; Zhu, X.; Shen, Y. Mutations in SCN9A, encoding a sodium channel a subunit, in patients with primary erythermalgia. *J. Med. Genet.* **2004**, *41*, 171–174. (f) Fab.; Vanhoutte, E. K.; Gerrits, M. M.; Dib-Haij, S.; Drenth, J. P.; Waxman, S G.; Merkies, I. S. Gain of function $Na_V1.7$ mutations in idiopathic small fiber neuropathy. *Ann. Neurol.* **2012**, *71*, 26–39.

(2) Ahuja, S.; Mukund, S.; Deng, L.; Khakh, K.; Chang, E.; Ho, H.; Shriver, S.; Young, C.; Lin, S.; Johnson, J. P., Jr.; Wu, P.; Li, J.; Coons, M.; Tam, C.; Brillantes, B.; Sampang, H.; Mortara, K.; Bowman, K. K.; Clark, K. R.; Estevez, A.; Xie, Z.; Verschoof, H.; Grimwood, M.; Dehnhardt, C.; Andrez, J. C.; Focken, T.; Sutherlin, D.

P.; Safina, B. S.; Starovasnik, M. A.; Ortwine, D. F.; Franke, Y.; Cohen, C. J.; Hackos, D. H.; Koth, C. M.; Payandeh, J. Structural basis of Nav1.7 inhibition by an isoform-selective small-molecule antagonist. *Science* **2015,** *350* , aac5464.

(3) McCormick, K.; Santos, S.; Chapman, M.L.; Krafte, D.S. Marron, B.E.; West, C.W.; Krambis, M.J.; Antonio, B.M.; Zellmer, S.G.; Printzenhoff, D.; Padilla, K.M.; Lin, Z.; Wagoner, P.K.; Swain, N.A.; Stupple, P.A.; de Groot, M.; Butt, R.P.; Castle, N.A. Voltage sensor interaction site for selective small molecule inhibitors of voltage-gated sodium channels. *PNAS*, 2013, *110*, 1-9.

(4) a) Bregman, H.; Berry, L.; Buchanan, J. L.; Chen, A.; Bu, B.; Feric, E.; Hierl, M.; Huang, L.; Immke, D.; Janosky, B.; Johnson, D.; Li, X.; Liguitti, J.; Liu, D.; Malmberg, A.; Matson, D.; McDermott, J.; Miu, P.; Nguyen, H. N.; Patel, V. F.; Waldon, D.; Wilenkin, B.; Zheng, X. M.; Zou, A.; McDonough, S. I.; DiMauro, E. F. Identification of a potent, state-dependent inhibitor of Nav1.7 with oral efficacy in the formalin model of persistent pain. *J. Med. Chem.* 2011, *54*, 4427–4445. b) Chakka, N.; Bregman, H.; Du, B.; Nguyen, H. N.; Buchanan, J. L.; Feric, E.; Ligutti, J.; Liu, D.; McDermott, J. S.; Zou, A.; McDonough, S. I.; Dimauro, E. F. Discovery and hit-to-lead optimization of pyrrolopyrimidines as potent, state-dependent $Na_v1.7$ antagonists. *Bioorg. Med. Chem. Lett.* 2012, *22*, 2052-2062. c) Nguyen, H. N.; Bregman, H.; Buchanan, J. L.; Du, B.; Feric, E.; Huang, L.; Li, X.; Ligutti, J.; Liu, D.; Malmberg, A. B.; Matson, D. J.; McDermott, J. S.; Patel, V. F.; Wilenkin, B.; Zou, A.; McDonough, S. I.; DiMauro, E. F. Discovery and optimization of aminopyrimidinones as potent and state-dependent Nav1.7 antagonists. *Bioorg. Med. Chem. Lett.* 2012, *22*, 1055-1060. d) Matson, D. J.; Hamamoto, D. T.; Bregman, H.; Cooke, M.; DiMauro, E. F.; Huang, L.; Johnson, D.; Li, X.; McDermott, J.; Morgan, C.; Wilenkin, B.; Malmberg, A. B.; McDonough, S. I.; Simone, D. A. Inhibition of inactive states of tetrodotoxin-sensitive sodium channels reduces spontaneous firing of C-fiber nociceptors and produces analgesia in formalin and complete freund's adjuvant models of pain. *PloS one* 2015, *10*, e0138140. d) Focken, T.; Liu, S.; Chahal, N.; Dauphinais, M.; Grimwood, M.E.; Chowdhury, S.; Hemeon, I.; Bichler, P.; Bogucki, D.; Waldbrook, M.; Bankar, G.; Sojo, L.E.; Young, C.; Lin, S.; Shuart, N.; Kwan, R.; Pang, J.; Chang, J.H.; Safina, B.S.; Sutherlin, D.P.; Johnson Jr. J.P.; Dehnhardt, C.M.; Mansour, T.S.; Oballa R.M.; Cohen, C.J.; Robinette.

C.L. Discovery of aryl sulfonamides as isoform-selective inhibitors of $Na_V1.7$ with efficacy in rodent pain models. *ACS Med. Chem. Lett.* 2016, *7*, 277-282. e) Wu, Y.; Guernon, J.; Shi, J.; Ditta, J.; Robbins, K.J.; Rajamani, R.; Easton, A.; Newton, A.; Bourin, C.; Mosure, K.; Soars, M.G.; Knox, R.J.; Matchett, M.; Pieschl, R.L.; Post-Munson, D.J.; Wang, S.; Herrington, J.; Graef, J.; Newberry, K.; Bristow, L.J.; Meanwell, N.A.; Olson, R.; Thompson, L.A.; Dzierba, C. Development of new benzenesulfonamides as potent and selective Nav1.7 inhibitors for the treatment of pain. *J. Med. Chem.* 2017*, 60,* 2513-2525. f) Roecker, A.J.**;** Egbertson, M.; Jones, K.L.G.; Gomez, R.; Kraus, R.L.; Li, Y.; Koser, A.J.; Urban, M.O.; Klein, R.; Clements, Daley, M.C.; Wang, J.; Finger, E.N.; Majercak, J.; Santarelli, V.; Gregan, I.; Cato, M.; Filzen, T.; Jovanovska, A.; Wang, Y.H.; Wang, D.; Joyce, L.A.; Sherer, E.C.; Peng, X.; Wang, X.; Sun, H.; Coleman, P.J.; Houghton, A.K.; Layton, M.E. Discovery of selective, orally bioavailable, N-linked arylsulfonamide Nav1.7 inhibitors with pain efficacy in mice. *Bioorg. Med. Chem. Lett.* **2017**, Ahead of print. g) For recent work in the area of peptide inhibition, please see: Murray, J.K.; Ligutti, J.; Liu, D.; Zou, A.; Poppe, L.; Li, H.; Andrews, K.L.; Moyer, B.D.; McDonough, S.I.; Favreau, P.; Stocklin, R.; Miranda, L.P. Engineering Potent and Selective Analogues of GpTx-1, a Tarantula Venom Peptide Antagonist of the NaV1.7 Sodium Channel *J. Med. Chem.* 2015*, 58,* 2299-2314.

(5) DiMauro, E. F.; Altmann, S.; Berry, L. M.; Bregman, H.; Chakka, N.; Chu-Moyer, M.; Feric Bojic, E.; Foti, R. S.; Fremeau, R. T., Jr.; Gao, H.; Gunaydin, H.; Guzman-Perez, A.; Hall, B. E.; Huang, H.; Jarosh, M.; Kornecook, T.; Lee, J.; Ligutti, J.; Liu, D.; Moyer, B. D.; Ortuno, D.; Rose, P. E.; Schenkel, L. B.; Taborn, K.; Wang, J.; Wang, Y.; Yu, V. L.; Weiss, M. M. Application of a parallel synthetic strategy in the discovery of biaryl acyl sulfonamides as efficient and selective $Na_V1.7$ inhibitors. *J. Med. Chem.* **2016**, *59*, 7818-7839.

(6) a) Marx, I.E.; Dineen, T.A.; Able, J.; Bode, C.; Bregman, H.; Chu-Moyer, M.; DiMauro, E.F.; Du, B.; Foti, R.S.; Fremeau Jr., R.T.; Gao, H.; Gunaydin, H.; Hall, B.E.; Huang, L.; Kornecook, T.; Kreiman, C.R.; La, D.S.; Ligutti, J.; Lin, M.J.; Liu, D.; McDermott, J.; Moyer, B.D.; Peterson, E.A.; Roberts, J.T.; Rose, P.; Wang, J.; Youngblood, B.D.; Yu, V.; Weiss, M.M. Sulfonamides as selective $Na_v1.7$ inhibitors: optimizing potency and pharmacokinetics to enable *in vivo* target engagement. *ACS Med. Chem. Lett.* **2016**, *7*, 1062-1067. b)

Graceffa, R.F.; Boezio, A.A.; Able, J.; Altmann, S.; Berry, L.M.; Boezio, C.M.; Butler, J.R.; Chu-Moyer, M.Y.; Cooke, M.; Di Mauro, E.F.; Dineen, T.A.; Feric Bojic, E.; Foti, R.S.; Fremeau, Jr., R.T.; Guzman-Perez, A.; Gao, H.; Gunaydin, H.; Huang, H.; Huang, L.; Ilch, C.; Michael Jarosh, Thomas Kornecook, Kreiman, C.R.; La, D.S.; Ligutti, J.; Milgram, B.C.; Lin, M.J.; Marx, I.E.; Nguyen, H.N.; Peterson, E.A.; Rescourio, G.; Roberts, J.; Schenkel, L.B.; Shimanovich, R.; Sparling, B.A.; Stellwagen, J.; Taborn, K.; Vaida, K.R.; Wang, J.; Yeoman, J.T.S.; Yu, V.L.; Zhu, D.; Moyer, B.D.; Weiss, M.M. Sulfonamides as Selective NaV1.7 Inhibitors: Optimizing Potency, Pharmacokinetics, and Metabolic Properties to Obtain Atropisomeric Quinolinone (AM-0466) that Affords Robust In Vivo Activity. *J. Med. Chem.* **2017**, Ahead of print. c) Weiss, M.M.; Dineen, T.A.; Marx, I.E.; Altmann, S.; Boezio, A.A.; Bregman, H.; Chu-Moyer, M.Y.; Di Mauro, E.F.; Feric Bojic, E.; Foti, R.S.; Gao, H.; Graceffa, R.F.; Gunaydin, H.; Guzman-Perez, A.; Huang, H.; Huang, L.; Jarosh, M.; Kornecook, T.; Kreiman, C.R.; Ligutti, J.; La, D.S.; Lin, M.J.; Liu, D.; Moyer, B.D.; Nguyen, H.N.; Peterson, E.A.; Rose, P.E.; Taborn, K.; Youngblood, B.D.; Yu, V.L.; Fremeau, Jr., R.T. Sulfonamides as Selective $Na_V1.7$ Inhibitors: Optimizing Potency and Pharmacokinetics While Mitigating Metabolic Liabilities. *J. Med. Chem.* 2017, Ahead of print.

(7) The vast majority of zwitterionic inhibitors were non-progressible due to poor pharmacokinetics. Compound **1** was a unique exception to this general trend. See reference 6.

(8) a) Gleeson, M.P. Generation of a Set of Simple, Interpretable ADMET Rules of Thumb. *J. Med. Chem.* **2008,** *51,* 817-834. b) Lovering, F.; Bikker, J.; Humblet, C. Escape from flatland: increasing saturation as an approach to improving clinical success. *J. Med. Chem.* **2009,** *52* , 6752-6756. c) Ritchie, T. J.; Macdonald, S. J. The impact of aromatic ring count on compound developability--are too many aromatic rings a liability in drug design? *Drug Discovery Today* **2009,** *14*, 1011-1020. d) Ritchie, T. J.; Macdonald, S. J.; Young, R. J.; Pickett, S. D., The impact of aromatic ring count on compound developability: further insights by examining carbo- and hetero-aromatic and -aliphatic ring types. *Drug Discovery Today* **2011,** *16*, 164-171.

(9) The LipE calculation is based upon clogP.

(10) (a) $Na_V1.7$ potency was measured using a Patch-Xpress (PX) electrophysiology assay conducted with a protocol that established ~20% inactivation and hence enabled the identification of state dependent inhibitors (b) PX IC_{50} determinations were made using at least four different concentrations of test compound at half log units applied individually, with washout, recovery of current, and resetting of holding voltage between each individual concentration. Percent inhibition as a function of compound concentration was pooled from at least n = 10 different cells, with two to three data points per concentration, and fitting the resulting data set with a Hill (4-parameter logistic) fit in DataXpress 2.0 software to produce a single IC_{50} curve. See Experimental for complete details of protocols.

(11) pKa values were calculated from capillary electrophoresis data obtained with pKa PRO Analyzer (AATI, Ames, IA) in the pH range of 1.7 to 11.2

(12) (a) Evans, D. C.; Watt, A. P.; Nicoll-Griffith, D. A.; Baillie, T. A. Drug-protein adducts: an industry perspective on minimizing the potential for drug bioactivation in drug discovery and development. *Chem. Res. Toxicol.* **2004**, *17*, 3–16. (b) Kalgutkar, A. S.; Gardner, I.; Obach, R. S.; Shaffer, C. L.; Callegari, E.; Henne, K. R.; Mutlib, A. E.; Dalvie, D. K.; Lee, J. S.; Nakai, Y.; O'Donnell, J. P.; Boer, J.; and Harriman, S. P. A comprehensive listing of bioactivation pathways of organic functional groups. *Curr. Drug Metab.* **2005**, *6*, 161–225. (c) Kalgutkar, A. S.; Soglia, J. R. Minimising the potential for metabolic activation in drug discovery. *Expert Opin. Drug Metab. Toxicol.* **2005**, *1*, 91–142.

(13) Both GX-936 and PF-04856264 first appeared in the following patent. Beaudoin, S.; Laufersweiler, M.C.; Markworth, C.J.; Marron, B.E.; Millan, D.S.; Rawson, D.J.; Reister, S.M.; Sasaki, K.; Storer, R.I.; Stupple, P.A.; Swain, N.A.; West, C.W.; Shulan, Z. Preparation of heteroarylsulfonamide derivatives for use as analgesics. WO 2010079443 A1, July 10, 2010.

(14) The tritiated ligand employed for the displacement assay: (*P*)-1-(3'-chloro-2-fluoro-5,5'-dimethoxy-[1,1'biphenyl]-4-yl)-*N*-(isoxazol-3-yl)-2-oxo-1,2-dihydroquinoline-6-sulfonamide[5'-methoxy-C^3H_3]; based upon compound 501 from the following patent: Boezio, C.; Boezio, A.; Bregman, H.; Chakka, N.; Coats, J. R.; Copeland, K. W.; DiMauro, E. F.; Dineen, T.; Gao, H.; La, D.; Marx, I. E.; Nguyen, H-N.; Peterson, E. A.;

Weiss, M. Dihydrobenzoxazine and tetrahydroquinoxaline sodium channel inhibitors. PCT Int. Appl. WO2013122897, Aug. 22. 2013.

(15) The X-ray ID for the protein structure employed is 5EK0 and the docking protocol was Schrodinger Glide with SP (standard precision).

(16) Percent homology was determined by comparison of the linear sequences and based upon identity of residue. This calculation was perform employing the Molecular Operating Environment (MOE) software.

(17) a) Le Bars, D.; Gozariu, M.; Cadden, S. W. Animal Models of Nociception. *Pharmacol. Rev.***2001**, *53*, 597–652. b) Bannon, A.W.; Malmberg, A.B. Unit 8.9 models of nociception: hot plate, tail flick, and formalin tests in rodents. *Curr. Protoc. Neurosci. 41*, 16.

(18) Liang, J., Brochu, R. M., Cohen, C.J.; Dick, I.E.; Felix, J.P.; Fisher, M.H.; Garcia, M.L.; Kaczorowski, G.J.; Lyons, K.A.; Meinke, P.T. Priest, B.T.; Schmalhofer, W.A.; Smith, M.M.; Tarpley, J.W.; Williams, B.S.; Martin, W.J.; Parsons, W.H. Discovery of potent and use-dependent sodium channel blockers for treatment of chronic pain. *Bioorg. Med. Chem. Lett.* **2005**, *15*, 2943–2947.

(19) The automated nature of this experiment makes this approach appealing as it removes operator bias in the quantitation of pain: Yaksh, T. L.; Ozaki, G.; McCumber, D.; Rathbun, M.; Svensson, C.; Malkmus, S.; Yaksh, M. C. An automated flinch detecting system for use in the formalin nociceptive bioassay. *J. Appl. Physiol.* **2001**, *90*, 2386–2402.

(20) Rat IV, 0.50 mg/kg, formulation: DMSO; Rat PO, 10 mg/kg, formulation: 30% (w/v) hydroxypropyl β-cyclodextrix in water pH adjusted to 10.0 with KOH

(21) Blair, N.T.; Bean, B.P. Roles of tetrodotoxin (TTX)-sensitive Na+ current, TTX-resistant Na+ current, and Ca2+ current in the action potentials of nociceptive sensory neurons. *J. Neurosci.* **2002**, *22*, 10277-10290

(22) Jarvis, M.F.; Honore, P.; Shieh, C.; Chapman, M.; Joshi, S.; Zhang, X.; Kort, M.; Carroll, W.; Marron, B.; Atkinson, R.; Thomas, J.; Liu, D.; Krambis, M.; Liu, Y.; McGaraughty, S.; Chu, K.; Roeloffs, R.; Zhong, C.; Mikusa, J.P.; Hernandez, G.; Gauvin, D.; Wade, C.; Zhu, C.; Pai, M.; Scanio, M.; Shi, L.; Drizin, I.; Gregg, R.; Matulenko, M.; Hakeem, A.; Gross, M.; Johnson, M.; Marsh, K.; Wagoner, P.K.; Sullivan, J.P.; Faltynek, C.R.;

Krafte, D.S. A-803467, a potent and selective Nav1.8 sodium channel blocker, attenuates neuropathic and inflammatory pain in the rat. *PNAS* **2007**, *104*, 8520-8525.

(23) Chimera work performed using chimeras made from human Nav1.7 and human Nav1.5 with **1** comparable to that reported by Pfizer revealed similarly that selective sulfonamide hNav1.7 inhibitors such as **1** were binding in the DIV voltage sensing domain. Further scrutiny of the protein sequence for the DIV domain and comparison of human and rat Nav1.7 and human Nav1.5 led to the hypothesis that our inhibitors were interacting across the S2 and S4 helices, in a manner likely similar to that reported for PF-04856264, which shows a similar selectivity profile to **1.**

(24) (a) Davidson, S.; Giesler, G.J. The Multiple Pathways for Itch and their interactions with Pain. *Cell* **2010** *33*, 550-558. (b) Devigili, G.; Eleopra, R.; Pierro, T.; Lombardi, R.; Rinaldo, S.; Lettieri, C.; Faber, C.G.; Ingemar, M.S.J.; Waxman, S.G.; Lauria, G. Paroxysmal itch caused by gain-of-function $Na_V1.7$ mutation. *Pain* **2014**, *155*, 1702-1707.

(25) Gingras, J.; Smith, S.; Matson, D. J.; Johnson, D.; Nye, K.; Couture, L.; Feric, E.; Yin, R.; Moyer, B. D.; Peterson, M. L.; Rottman, J. B.; Beiler, R. J.; Malmberg, A. B.; McDonough, S. I. Global Nav1.7 knockout mice recapitulate the phenotype of human congenital indifference to pain. *PloS One* **2014,** *9*, e105895.

(26) Rats do not respond to a histamine challenge and therefore the focus of this investigation was on mouse.

(27) **15** didn't demonstrate any significant binding to H1, 2 or 3 in a Cerep panel (single point displacement @ 10 μM).

Graphical Abstract

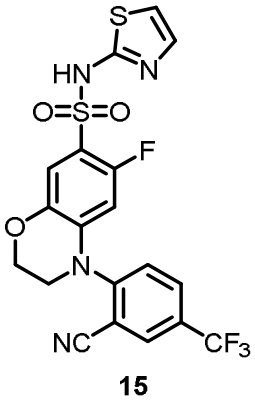

15